Chapter 5

Size dependent Activity of Carbon-based Fullerenes with L-leucine

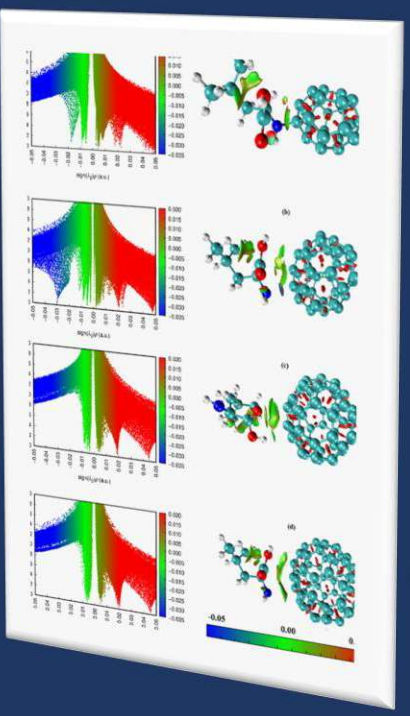

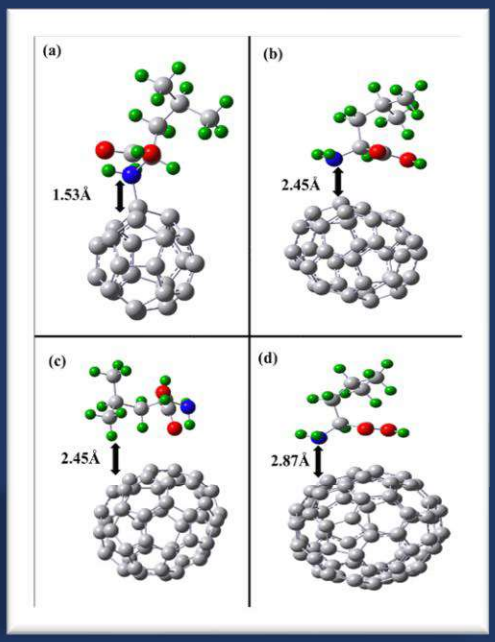

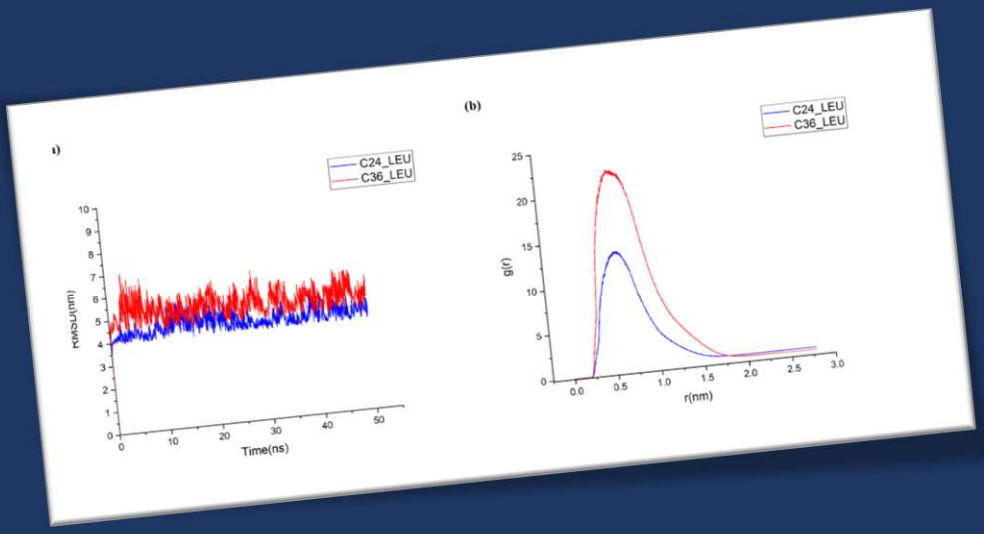

5.1 Introduction

Fullerenes have garnered significant admiration in the realm of science, and their appeal extends beyond their aesthetic qualities. They possess a multitude of distinctive attributes, particularly their ability to function as electron acceptors in both solid and liquid phases, setting them apart[1]. Following Kroto et al.'s groundbreaking discovery of macroscopic-scale C_{60} synthesis, fullerenes rapidly pivoted towards the creation of functional systems, with a keen emphasis on potential applications[2]. Graphite aspires to possess the qualities found in fullerenes, driven by the curvature resulting from the presence of pentagons[3]. Fullerene derivatives have exhibited a diverse range of physical attributes that render them attractive for applications in materials[4], pharmaceuticals[5], and biological research[6]. According to the Isolated Pentagon Rule (IPR), fullerenes of the same size but with non-IPR isomers are comparatively less stable than their IPR counterparts[7]. The C_{70} fullerene, characterized by D_{5h} symmetry, stands as the second smallest member within the Isolated Pentagon Rule (IPR) fullerene family, while the C_{60}, featuring I_h symmetry, claims the title of the smallest member[8]. Interestingly, it has been unveiled that specific sites within the second-most prevalent IPR fullerene, C_{70}, exhibit higher reaction energies compared to those in C_{60} and boast a greater binding energy per atom[9-10]. In a groundbreaking study that clinched the Nobel Prize, not only were C_{60} and C_{70} identified as exceptional clusters with heightened mass spectrometry signals, but C_{50} also made a significant appearance[11] . While C_{60} and C_{70} have been extensively studied and are widely accessible, the experimental data on C_{50} is notably scarce[11-12]. Furthermore, C_{50} conforms to Hirsch's electron counting rule for spherical molecules ($2(N + 1)^2$), which implies a high expected aromatic nature[13-14]. It's worth emphasizing that C_{50} represents the smallest carbon structure that lacks three pentagons directly or consecutively connected, potentially rendering it less flexible compared to its smaller fullerene counterparts.

Contrasting with its smaller fullerene counterparts, C_{50} stands out with its anticipated heightened aromaticity and reduced strain energy. Consequently, C_{50} has been traditionally considered the prime candidate for producing fullerenes smaller than C_{60}[13][15]. Another notable member of the non-Isolated Pentagon Rule (IPR) family, the experimentally synthesized C_{36} fullerene, has garnered substantial scientific attention due to the inclusion of fused five-membered rings, which imparts significant strain and reactivity to the molecule[16-17]. Extensive theoretical studies have delved into the structural and electrical properties of C_{36}

fullerene and its derivations[18-20]. In the scope of our own research, we have broadened our investigation to include C_{24}, which ranks as the second smallest member in the fullerene family, alongside our exploration of various other selected fullerenes. Among these, the C_{24} fullerene, possessing D_{6h} symmetry, has emerged as the most stable within its class and has found practical applications in fields such as drug delivery[21-22] , biosensing[6] , hydrogen storage[23] , Li-ion batteries[24] , and more. An essential scientific frontier within the realms of both material science and physical chemistry lies in the art of bridging the gap between biomolecules and organic materials, a fundamental requirement for advancing the development of biosensors with enhanced selectivity[25-26]. Recent strides in our understanding of the underlying physical mechanisms governing interactions between biomolecules and fullerenes have led to the creation of fullerene-based biosensors, poised to make significant contributions to biomedicine and related disciplines[27-28]. The utilization of fullerene-C_{60} has been recognized as an effective immobilization platform for DNA-antibody hybrids and protein hybrids in the context of electrochemical biosensors[28]. Amino acids, on the other hand, assume a foundational role in protein synthesis within the human body, influencing a multitude of vital biological processes. Consequently, the profound importance of comprehending protein structure becomes apparent, as it provides valuable insights into their biological functions and contributes significantly to the comprehension of innovative disease diagnoses and therapeutic strategies[29-30]. Notably, among the essential amino acids, L-leucine (LEU) stands out due to its unique status as one of the 20 amino acids that the human body cannot synthesize, necessitating its acquisition from dietary sources, underscoring its critical role. L-leucine holds substantial importance owing to its pivotal contributions to various physiological processes, including protein synthesis[31], cellular energy generation[32] , blood sugar regulation[33] , immune system integrity[34] , and the maintenance of neurological well-being[35], among others. However, deviations from normal L-leucine levels can serve as indicators of specific metabolic disorders. For example, elevated concentrations of L-leucine in the bloodstream may raise suspicion of maple syrup urine disease (MSUD), a rare genetic condition that hampers the body's capacity to metabolize branched-chain amino acids, including L-leucine[36]. Hence, there is a need to create sensors that can identify and measure L-leucine levels in biological specimens, offering valuable insights for researchers, healthcare experts, and individuals seeking to enhance their dietary choices. Numerous biophysical and chemical nano techniques have the potential to aid in the assessment of protein structures and compositions[29].

Surprisingly, as far as our knowledge extends, no prior investigations have explored the suitability of C_{70}, C_{50}, C_{36}, and C_{24} fullerenes as potential sensors for detecting L-leucine (LEU). This article employs Density Functional Theory (DFT) analysis to delve into the mechanisms underlying the heightened interactions between size-variable fullerenes like C_{70}, C_{50}, C_{36}, and C_{24} with L-leucine (LEU). Furthermore, through DFT examination, we conduct a comprehensive exploration of electronic properties, encompassing analysis of Natural Bond Orbitals (NBO), Mulliken charge, Density of States (DOS), and Real Space Density (RDG). We have used DFT calculations to investigate the binding kinetics and sensitivity of L-leucine to the mentioned fullerenes in both gas and solvent phases. Furthermore, we explore the solvent effect. Lastly, we employ classical molecular dynamics simulations to validate the stability of l-leucine and fullerene complexes, along with the dynamics of bond formation and breaking, under ambient conditions (310K) in an aqueous environment.

5.2 Computational Details

5.2.1 Details of DFT calculation

To perform structural optimization of L-leucine and fullerenes, as well as electronic calculations, we employed the DFT/B3LYP technique with the 6-311G(d,p) basis set and incorporated Grimme's dispersion correction[37] (D3 version) using the Gaussian 09 package[38]. The adsorption energy, denoted as Ead, is defined as follows:

$$E_{ad} = E_{fullerens/LEU} - (E_{fullerens} + E_{LEU}) \text{ .....(1)}$$

In this context, $E_{fullerene}$ represents the energy of the optimized fullerenes, while E_{LEU} and $E_{fullerens/LEU}$ denote the energies of the isolated L-leucine and the optimized fullerenes with adsorbed L-leucine, respectively. The energy gap between the Highest Occupied Molecular Orbital (HOMO) and Lowest Unoccupied Molecular Orbital (LUMO), known as the HOMO-LUMO energy gap (EG), is defined as

$$E_G = E_{LUMO} - E_{HOMO} \text{ .....(2)}$$

5.2.2 Details of Molecular Dynamics Simulation

We employed the GROMACS software, version 5.0.2[39], along with the CHARRM27 force field[40], to conduct classical molecular dynamics simulations. These simulations aimed to validate the adsorption behavior of the L-leucine (LEU) biomolecule on the external surface of fullerenes, including C_{36} and C_{24}. To achieve this, we constructed two simulation systems:

C_{36}/LEU and C_{24}/LEU. **Table 5.7** provides detailed information about all the systems subjected to examination. The water molecule was represented using the TIP3P model[41]. The MD simulation utilized the optimized structures from DFT calculations as its initial input, and these structures were converted into PDB format using GaussView 5.0. To account for periodic boundary constraints, all simulation boxes were made large enough to eliminate interactions between components and their neighboring cells. It's worth noting that in each enclosure, the biomolecules are positioned approximately 1.5 to 2 Å away from the surfaces of the fullerenes. The systems underwent an initial step of comprehensive minimization before attaining equilibrium, achieved through NVT and NPT ensembles for 100 ps each. The maintenance of a constant temperature of 310 K and pressure at 1 bar was ensured using the V-rescale and Berendsen algorithms, respectively[42]. For each system, production MD simulations were conducted, employing a time step of 2 femtoseconds, spanning 50 nanoseconds under periodic conditions. The LINCS method was utilized to constrain all bonds to their equilibrium lengths[43]. Long-range electrostatic interactions were managed through the particle-mesh Ewald (PME) approach, incorporating a 1.2 nanometer range cut-off for non-bonded interactions[44]. Molecular visualization was achieved using the Visual Molecular Dynamics (VMD) software[45].

5.3 Results and Discussion

5.3.1 DFT calculation results

5.3.1.1 Geometry Optimization of the adsorbent C_{24}, C_{36}, C_{50}, C_{70} fullerene and L-leucine (LEU)

To gain a comprehensive understanding of biosensor functionality, it is crucial to explore the structural and electronic attributes of both fullerenes and the biomolecule L-leucine (LEU). In this study, we began by optimizing all the considered fullerenes (C_{70}, C_{50}, C_{36}, and C_{24}) in conjunction with the biomolecule L-leucine (LEU), as illustrated in **Figure 5.1**. It's noteworthy that the first two selected fullerenes, C_{70} and C_{50}, belong to the D_{5h} point group, while the other two fullerenes, C_{36} and C_{24}, are characterized by the D_{6h} point group.

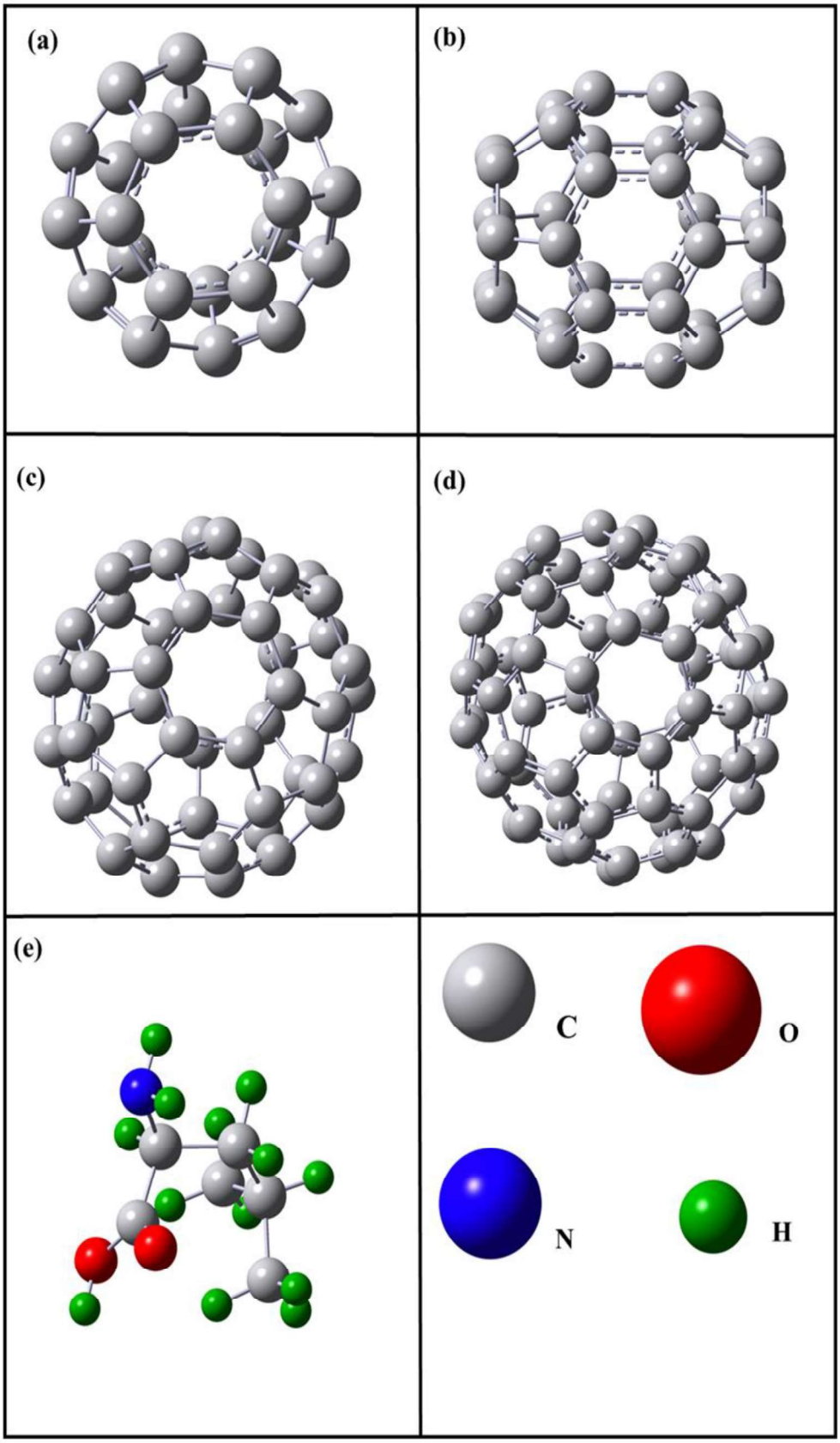

Figure 5.1: *Optimized structure of (a) C_{24},(b)C_{36},(c)C_{50} ,(d) C_{70} fullerene and (e) L-Leucine (LEU)*

The computed bond lengths and HOMO-LUMO gap (E_G) values for the fullerenes are presented in **Table-5.1**. It was observed that the E_G values for the chosen fullerenes, namely C_{70}, C_{50}, C_{36}, and C_{24}, are 1.83, 1.13, 1.30, and 2.68 eV, respectively. These findings align with prior research[5-6][45-48]. Additionally, **Table-5.1** contains the calculated cohesive energies

Table 5.1: *Calculated Values of HOMO-LUMO gap (E_G), cohesive energy (E_B), and Bond length of C_{24},C_{36},C_{50} and C_{70} fullerene.*

System	E_{LUMO} (eV)	E_{HOMO} (eV)	E_G (eV)	E_B in eV/atom	C-C in Å	C=C in Å
C_{24}	-4.22	-6.05	1.83	-6.93	1.46	1.36
C_{36}	-4.46	-5.59	1.13	-8.45	1.49	1.44
C_{50}	-4.57	-5.87	1.30	-8.66	1.45	1.38
C_{70}	-3.66	-6.34	2.68	-8.82	1.46	1.43

for these fullerenes. Their negative and high cohesive energy levels provide stability for them. The vibrational modes have also been studied to confirm stability with infrared (IR) spectrum frequencies. All of the vibration modes of the chosen fullerenes, according to our research, have actual frequencies between 400 and 1600 cm^{-1}. We found that all of the vibration modes of the selected fullerenes had actual frequencies that range between 400 and 1600 cm^{-1} (**Figure 5.2**). **Figure 5.3** shows the electron density distributions for the HOMO and LUMO orbitals of the selected fullerenes. In contrast to C_{50} and C_{70} fullerenes, we immediately observed a considerable localization of HOMO and LUMO electron concentrations in the peripheries of C_{24} and C_{36} fullerenes. After confirming the ground state characteristics of the relevant fullerenes, we optimised the LEU biomolecule[49-50] .

In order to pinpoint the perfect position where the greatest likelihood of contact may take place, we performed ESP (Electro Static Potential) mapping. **Figure 5.4** displays the charge distribution of the systems and the L-leucine. With neutral zones in between, red areas denote attractive potential or negative potential regions with the maximum electron density, and blue areas, electron deficiency or positive potential regions. Both the C_{24} and C_{36} fullerenes have the intermediate negative sections that span both empty areas and the blue region for the repulsive potential. In the case of C_{50} and C_{70}, the core region of the fullerenes has demonstrated repulsive potential. In the LEU biomolecule, the oxygen and nitrogen atoms both contain potent

negative electron regions. When LEU and the corresponding fullerenes are reoptimized in aqueous phase, there are no discernible changes.

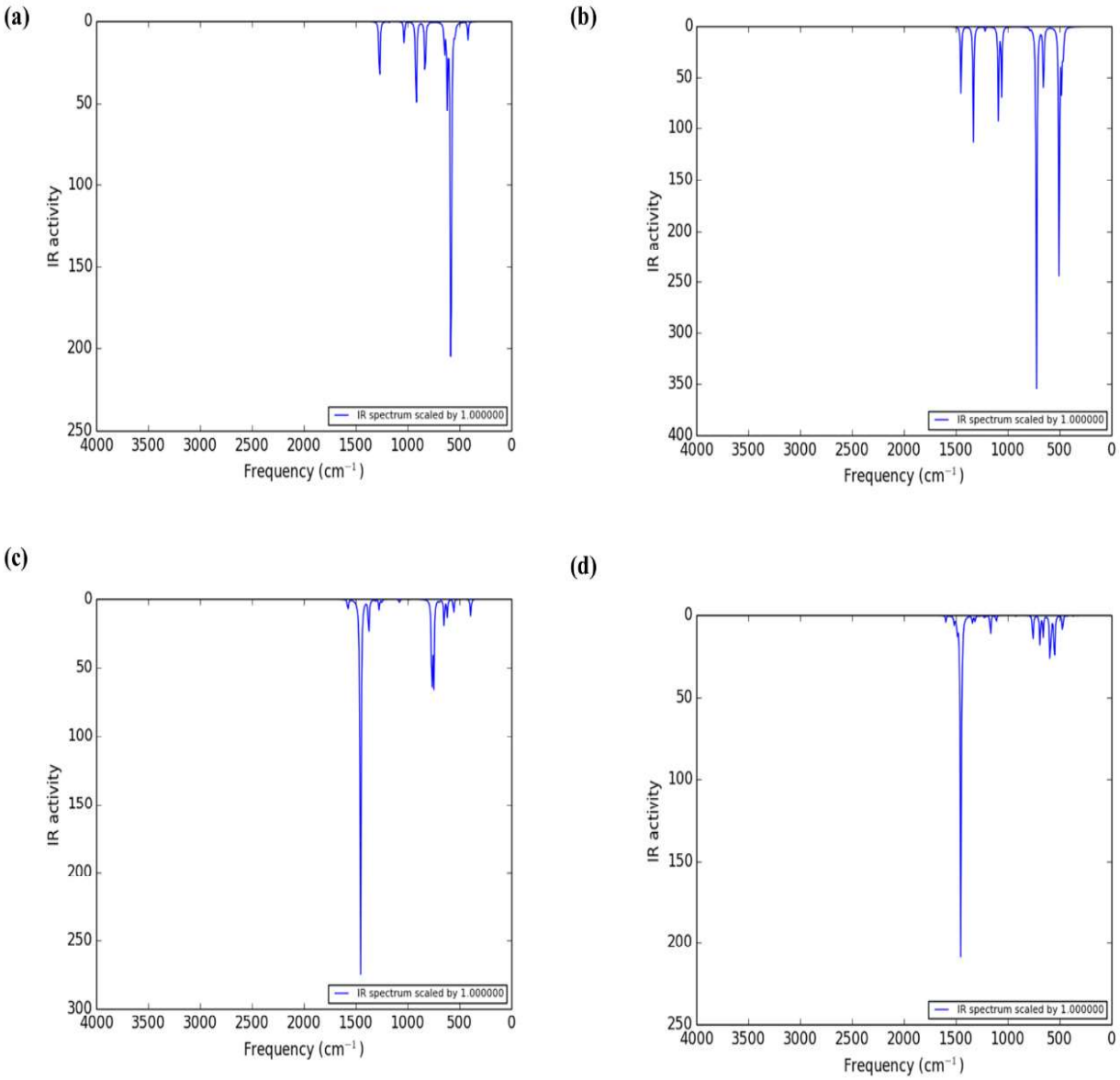

Figure 5.2: *IR of (a) C_{24},(b)C_{36},(c)C_{50} and (d) C_{70} fullerene*

5.3.1.2 Adsorption properties of L-leucine (LEU) molecule over C_{24}, C_{36}, C_{50} and C_{70}

In order to confirm the LEU biomolecule's binding affinity for particular fullerenes, we looked into its most stable shape when interacting with them (**Figure 5.5**). The LEU

biomolecule interacts with the fullerenes without incurring any structural modification, according to observations. Fullerenes' hexagonal or pentagonal rings serve as a platform for biomolecule interaction mechanisms. In order to identify the least energy conformer, a number of possible sites for the biomolecule to adsorb onto fullerenes have been investigated.

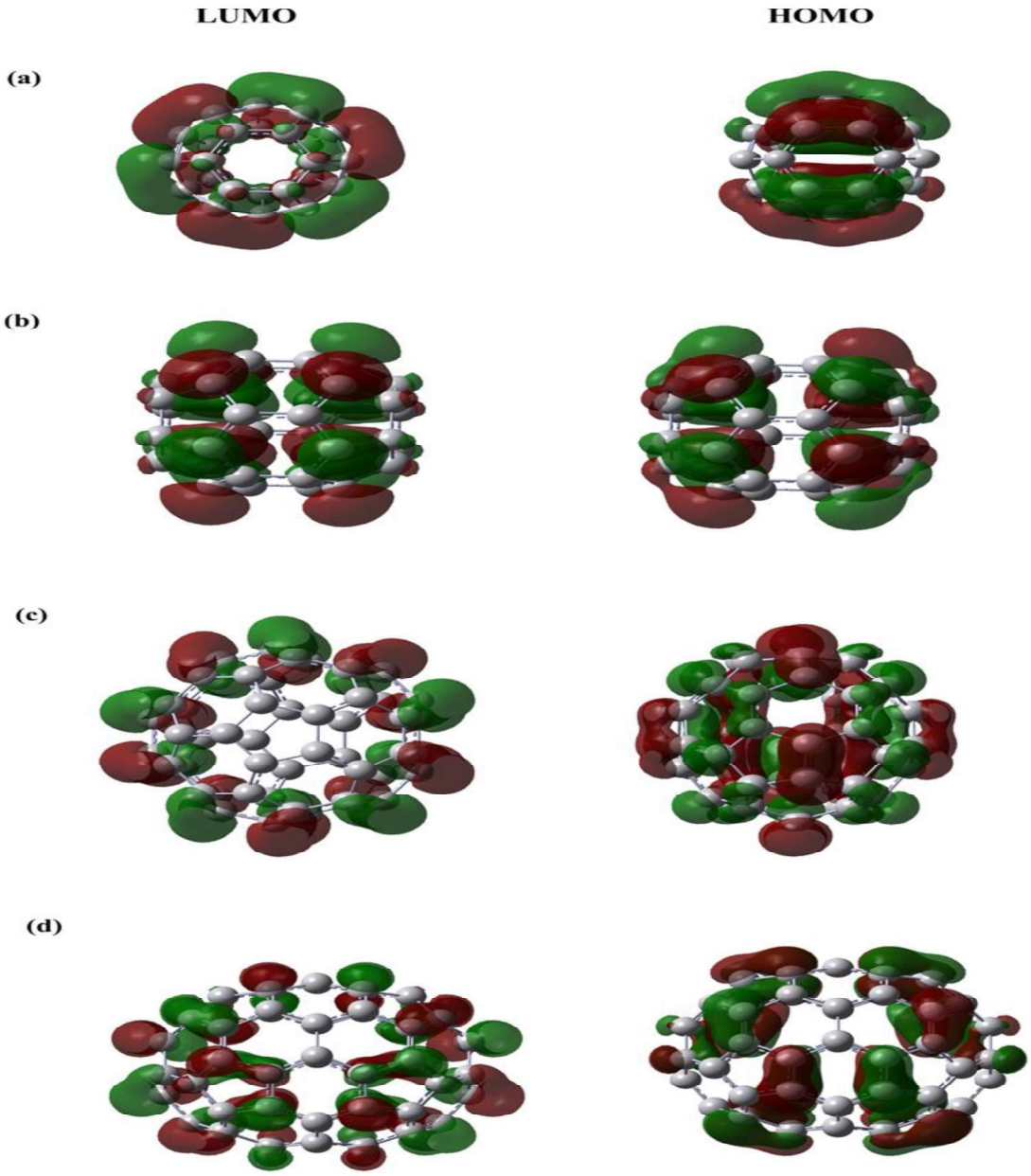

Figure 5.3 : *LUMO and HOMO electron contribution of (a) C_{24},(b)C_{36},(c)C_{50} and (d) C_{70} fullerene*

LEU is adsorbed across the hexagonal ring of the C_{36} fullerene with an energy of -0.35 eV. LEU biomolecule and C_{36} fullerene have an optimum separation of 2.45 Å, illustrating the physisorption characteristic of LEU. Physical adsorption of the LEU at energies of -0.33 eV and -0.36 eV, respectively, onto the hexagonal sites of C_{50} and C_{70} fullerenes has been observed[6]. At the smallest atomic distance, LEU is separated from the C_{50} and C_{70} fullerenes by 2.45 Å and 2.87 Å atoms, respectively (**Table 5.2**). The kind, order, or tendency of the biomolecules towards the fullerene

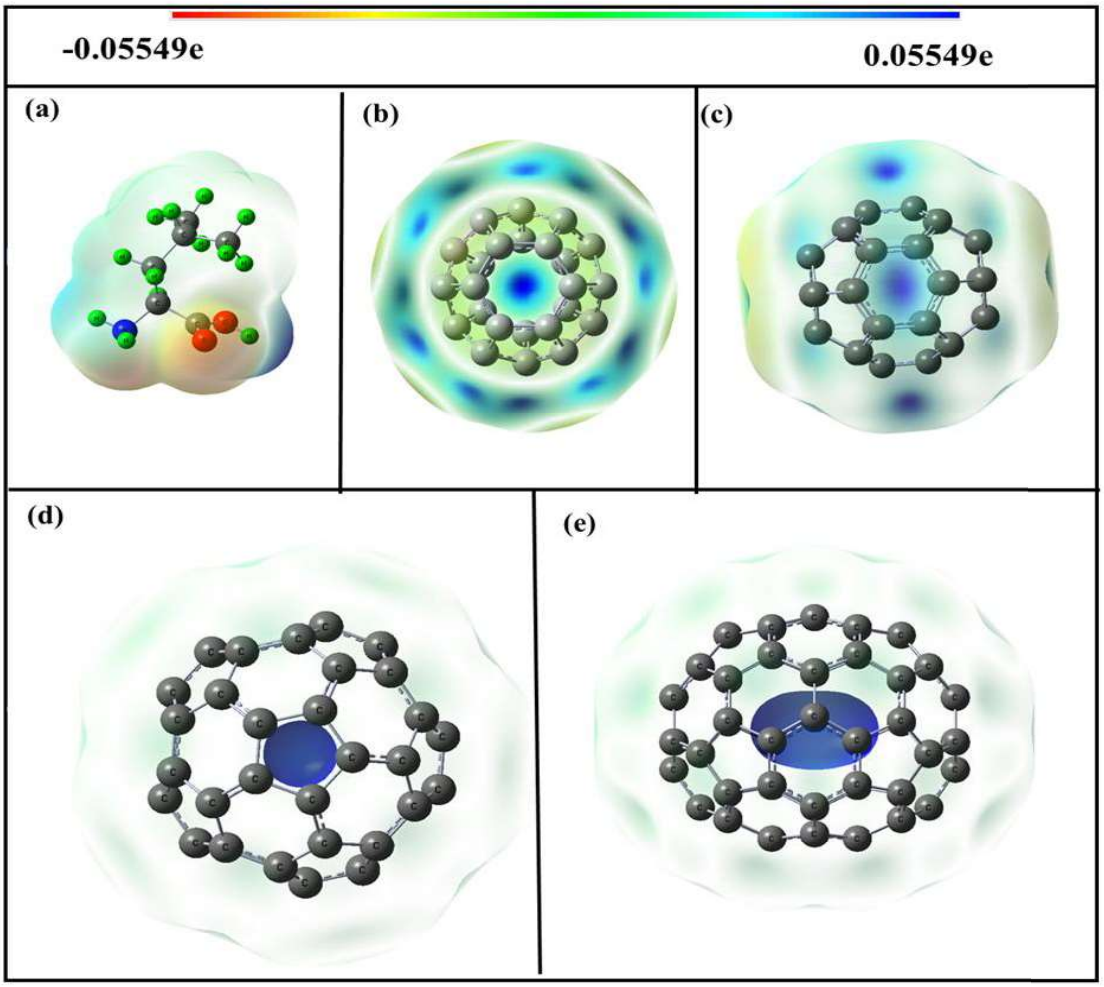

Figure 5.4: *ESP of (a) L-Leucine (LEU (b) C_{24},(c)C_{36},(d)C_{50} ,and (e) C_{70} fullerene (EPS) from -0.05549e to 0.05549e)).*

is revealed by the adsorption energies. We used NBO analysis and Mulliken charge analysis to study how quantum mechanics could be able to explain the biomolecules' propensity for fullerenes.

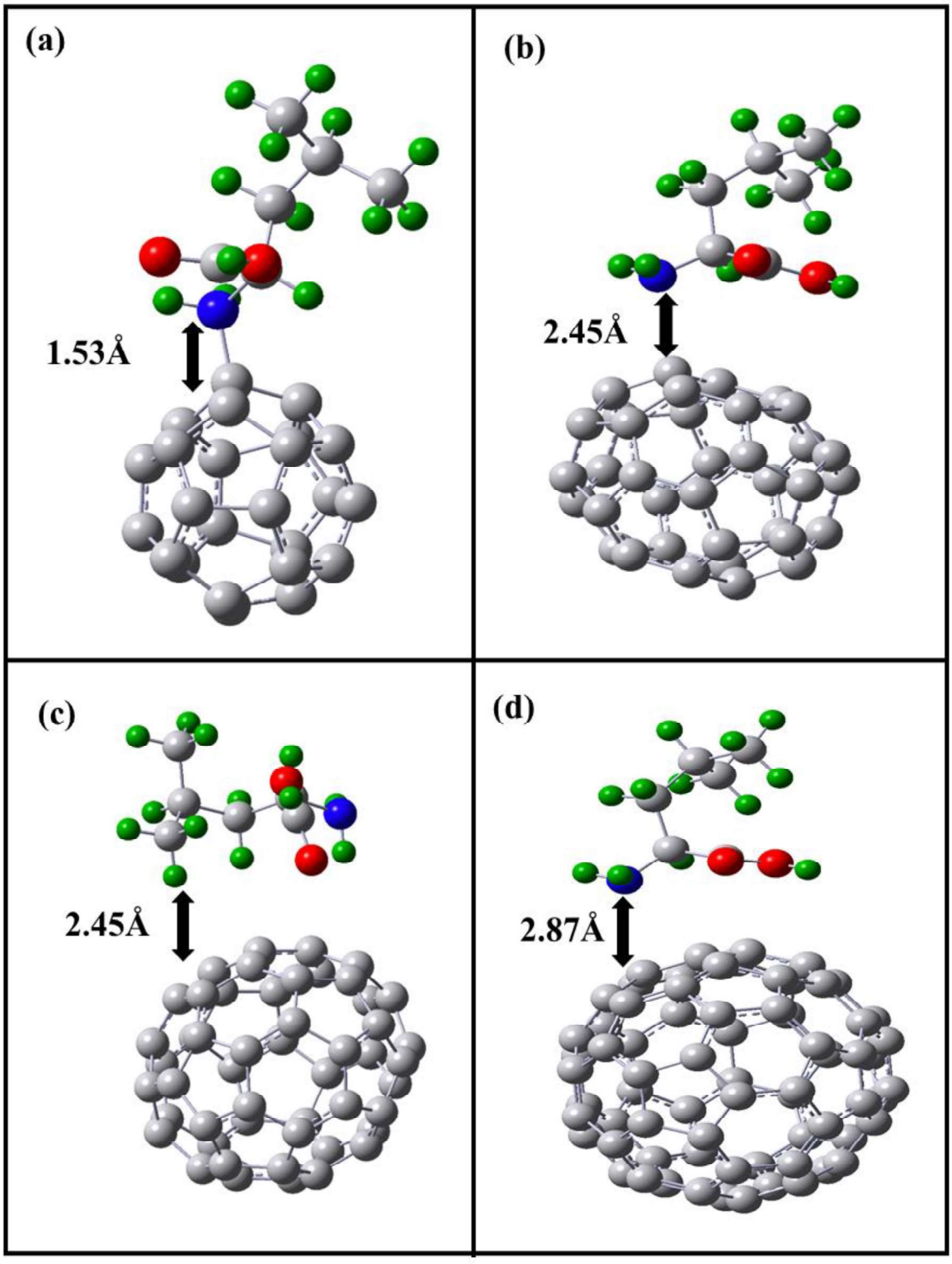

Figure 5.5: *Minimum energetic geometry of LEU adsorbed over (a) C_{24},(b)C_{36},(c)C_{50} and (d) C_{70} fullerene respectively.*

Table 5.2: *Calculated value of Adsorption energy (E_{ad}), LUMO energy (E_{LUMO}), Fermi level (E_F), HOMO energy (E_{HOMO}), HOMO-LUMO gap (E_G), relative change in E_F (ΔE_{FR}), relative change in E_G (ΔE_{GR}) and adsorption distance(d) of LEU adsorbed over C_{24},C_{36},C_{50} and C_{70} fullerene, respectively.*

System	E_{ad} (eV)	E_{LUMO} (eV)	E_F (eV)	E_{HOMO} (eV)	E_G (eV)	ΔE_{FR} (%)	ΔE_{GR} (%)	d (Å)
C_{24}/LEU	-1.14	-2.93	-3.88	-4.82	1.89	24.51	3.28	1.53
C_{36}/LEU	-0.35	-4.03	-4.58	-5.13	1.1	8.94	-2.65	2.45
C_{50}/LEU	-0.33	-4.55	-5.21	-5.87	1.32	0.19	1.53	2.45
C_{70}/LEU	-0.36	-3.55	-4.89	-6.22	2.67	2.2	-0.37	2.87

5.3.1.3 The natural bond orbital (NBO) charge analysis:

The electronic charge transfer, which is an important feature, allows us to better understand how an adsorbate interacts with an adsorbent. The charge transfer that takes place between certain fullerenes and biomolecules in their optimal geometrical configurations during the adsorption process may be explained by the NBO analysis, which is shown in **Table 5.3**[51].For the interactions between fullerenes and biomolecules, we also looked at the Mulliken population to determine the direction of spontaneous charge flow [52]. The LEU biomolecule's net Mulliken charge is determined to be +0.545e, +0.146e, +0.012e, and +0.027e, respectively, based on adsorption onto C_{24}, C_{36}, C_{50}, and C_{70} adsorbates. Since the isolated biomolecule has no net Mulliken charge, the positive values of the biomolecule's Mulliken charge in each case indicate that the charge has been transferred from the LEU to the fullerene[52-53] . In **Figure 5.6,** the charge distribution of LEU adsorbed onto certain fullerenes is displayed. The second-order Fock matrix predicted a donor-acceptor (bond-antibond) interaction between the chosen fullerenes and LEU. The NBO calculation has been utilised to explain the second-order perturbation stabilisation energy, $E^{(2)}$. The second order perturbation stabilisation energy, $E^{(2)}$, is expressed as [52] for the delocalization of the donor (i) to the acceptor (j)

$$E^{(2)} = \Delta E_y = q_i \frac{F^{(2)}(ij)}{\varepsilon_i - \varepsilon_j} \quad \ldots\ldots\ldots\ldots (3)$$

It is well known that the second order perturbation stabilization energy is related to the NBO interacting intensity and that higher donor-acceptor interactions lead to higher stabilization

energies, which give better stability for fullerene/biomolecule complexes[54] . **Table 5.3** in this instance only displays the highest values of $E^{(2)}$. The intermolecular interaction of the LEU/C_{24} complex suggests that (N27-H44) of the LEU serves as the acceptor and (C21-C24) of the C_{24}

Table 5.3: *The NBO second-order perturbation energy (E^2, kcal/mol) corresponds to the charge transfer between the LEU and C_{24},C_{36},C_{50} and C_{70} fullerene, respectively.*

System	Donor	Acceptor	E^2 (Kcal/mol)
C_{24}/LEU	BD(C21-C24)	BD*(N27-H44)	50.47
C_{36} /LEU	LP(N39)	LP*(C33)	15.09
C_{50}/LEU	BD*(C11-C12)	BD*(O51-H72)	12.80
C_{70}/LEU	BD(C32-C36)	BD*(O72-C79)	18.12

fullerene acts as the donor, which is consistent with the ESP results, according to the data that have been collected. The maximum value of $E^{(2)}$, 50.47 kcal/mol, indicates the greatest contact between the C_{24} fullerene and the LEU biomolecule. Indicating chemisorption as the adsorption process, LEU adsorption over C_{24} fullerene displays a charge transfer and high adsorption energy. The maximum $E^{(2)}$ values for the complexes of C_{36}/LEU, C_{50}/LEU, and C_{70}/LEU are respectively 15.09, 12.80, and 18.12 Kcal/mol. The reduced culminates in comparison to LEU/C_{24} complex support the physisorption nature of the adsorption between them. In basic words, it may be argued that the bulk of interaction occurs in the orbitals of pristine fullerenes, which serve as donors, and the π^* orbitals of LEU, which operate as acceptors.

5.3.1.4 Density of States (DOS)

An obvious indication that the LEU and systems have interacted is the change in HOMO and LUMO levels that occurs after the engagement, which triggers the charge transfer process. The density of states (DOS) analysis and data plotting were done using the Gaussum sofware, and the resulting images are shown in **Figure 5.7**. The HOMO and LUMO energies, as well as variations in the fermi level and band gap fluctuation in percent, are computed, as seen in **Table 5.2.** After the LEU is adsorbed onto C_{24} fullerene, the HOMO and LUMO

energies of fullerene change from -6.05 eV and -4.22 eV to -4.82 eV and -2.93 eV, respectively, indicating a 3.28% increase in the HOMO-LUMO gap.

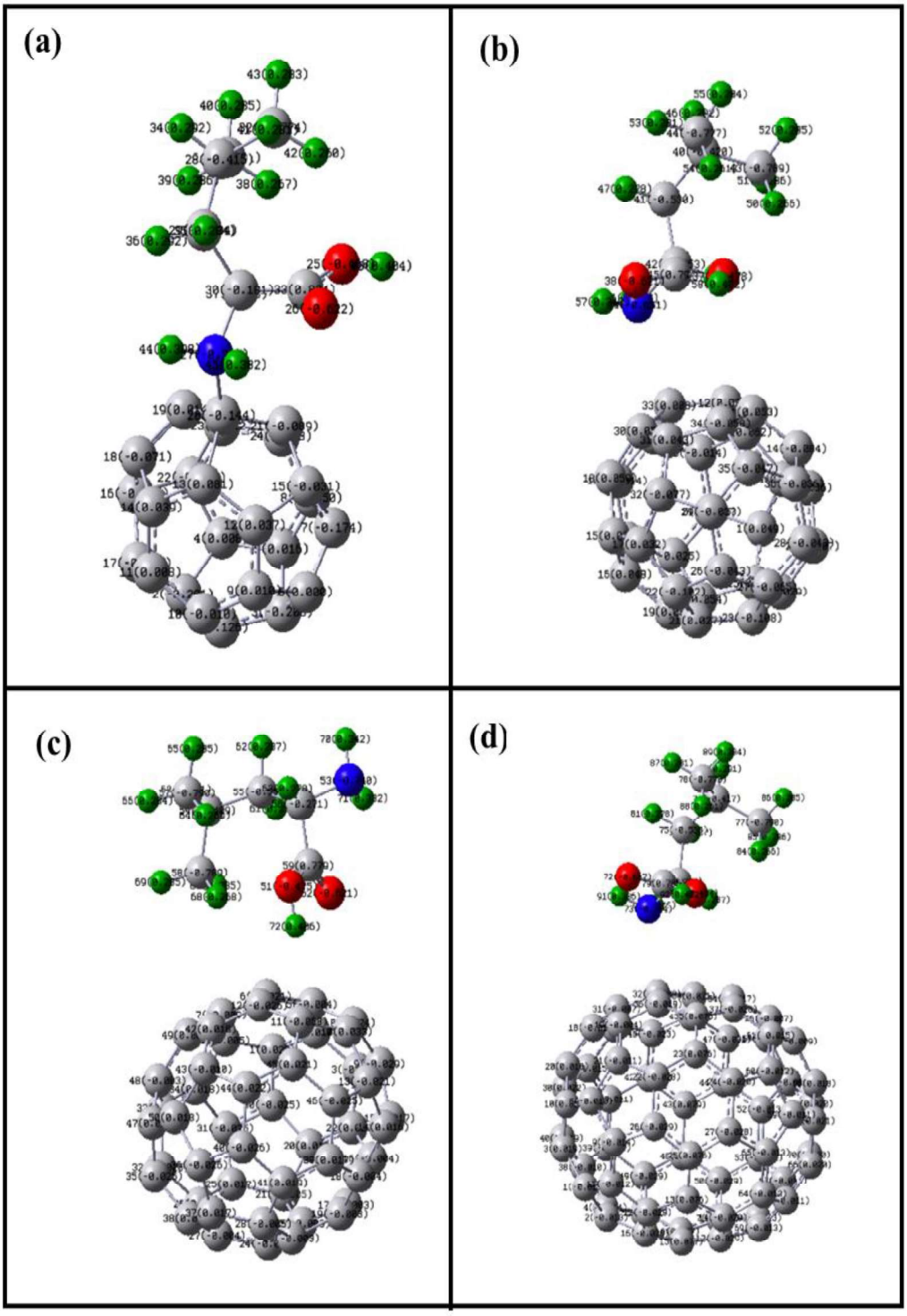

Figure 5.6: *Mulliken charge population analysis of LEU adsorbed over (a) C_{24},(b)C_{36},(c)C_{50} and (d) C_{70} fullerene respectively.*

Additionally, the C_{36} fullerene's HOMO-LUMO energy levels are -5.59 eV and -4.46 eV, respectively, and when the fullerene interacts with LEU, these levels fall to -5.13 eV and -4.03 eV, shifting the HOMO-LUMO gap by 2.65%. Similar changes have been made to the HOMO LUMO energy levels of the LEU/C_{50}, which have been changed from -5.87 eV and -4.57 eV to -5.87 eV and -4.55 eV, respectively. After LEU has been adsorbed on C_{70} fullerene, the HOMO-LUMO gap has not changed abruptly in any way. The C_{24}/LEU combination differs most from all other complexes in terms of E_G and E_F, suggesting that there is chemisorption between them. The localization of the LUMO electron density in **Figure 5.8** indicates the relationship between the nitrogen atom of the LEU biomolecule and the nearest carbon atom of the C_{24} fullerene. Due to the strong interaction between LEU and C_{24} fullerene, this occurrence demonstrates the existence of a chemical bond. The ideal adsorption energy between the C_{36}, C_{50}, and C_{70} fullerenes may be found by localizing the HOMO and LUMO electron densities for the LEU adsorbed over each of those materials.

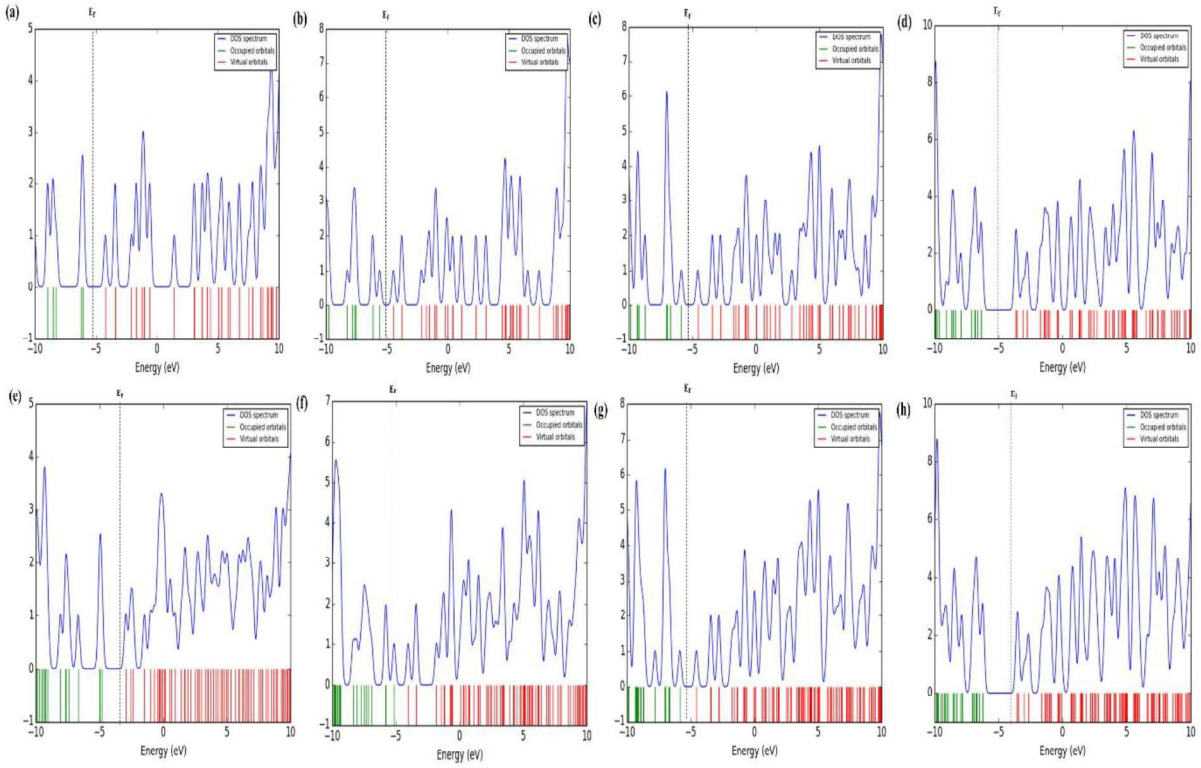

Figure 5.7: *Density of states of (a) C_{24},(b)C_{36},(c)C_{50} , and (d) C_{70} fullerene, (e) C_{24}/LEU,(f)C_{36} /LEU, (g)C_{50}/LEU and (h)C_{70}/LEU respectively.*

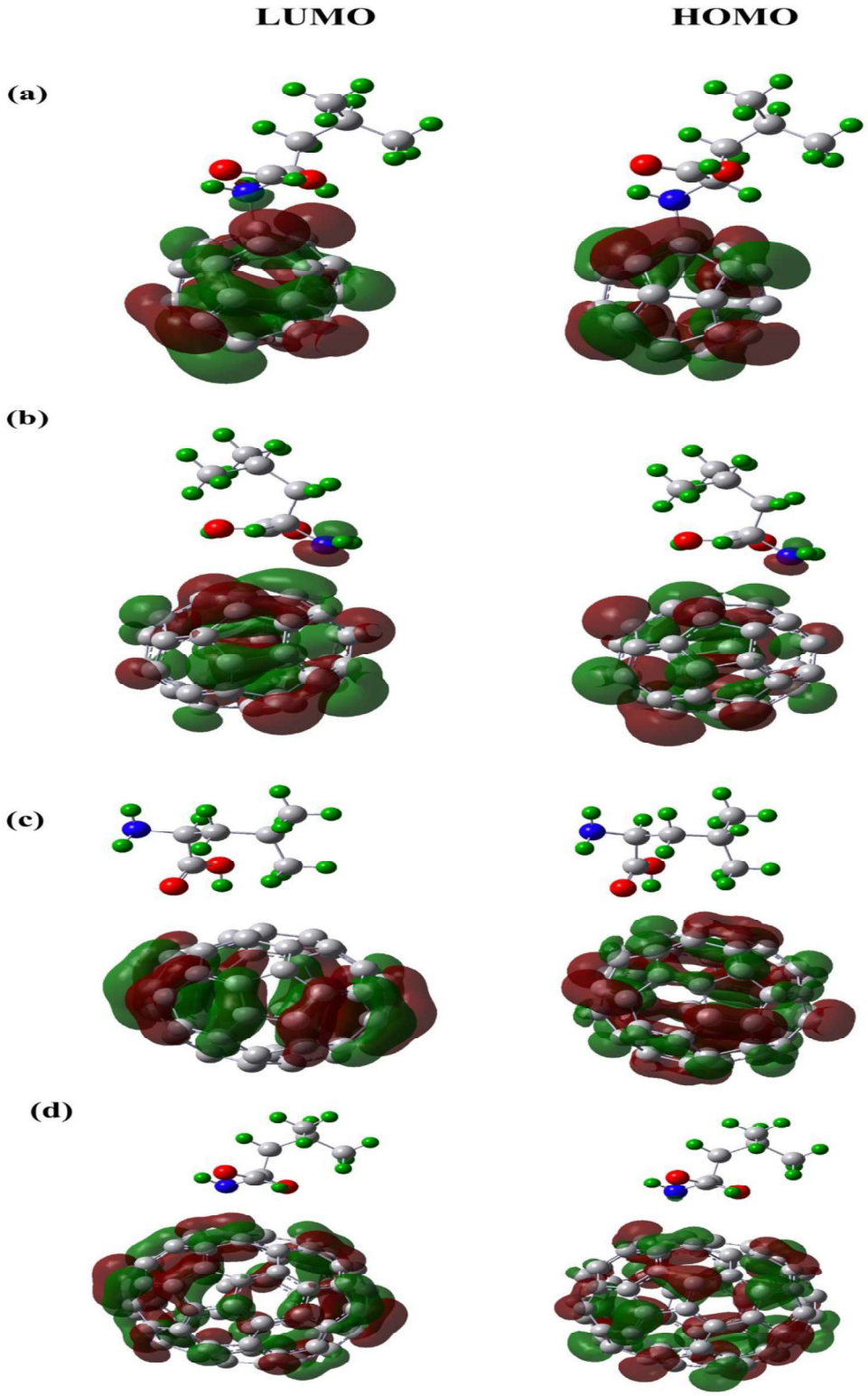

Figure 5.8: *The LUMO and HOMO electron density of LEU adsorbed over the pristine (a) C_{24},(b)C_{36},(c)C_{50} , and (d) C_{70} fullerene, respectively.*

5.3.1.5 RDG analysis

To gain insight into the attractive and repulsive forces at play and to characterize the nature of interactions within the LEU/fullerene complexes, Figure 8 illustrates scatter plots featuring the reduced density gradient (RDG) against the sign $(\lambda_2)\rho$, alongside non-covalent interaction (NCI) isosurfaces[55]. Stronger attractive connections, such as H-bonds and dipole-dipole interactions, are suggested by larger negative values of sign(λ2) with charge density (ρ) = -0.04, whereas strong steric interactions are indicated by positive values of sign(λ2) with(ρ) = 0.04. Furthermore, the Van der Waals (vdW) forces are almost ρ equal to 0[56]. Plots of NCI isosurfaces indicate that blue regions represent strong interactions, red regions a strong steric influence, and green regions vdW interactions. **Figure 5.9(a)** illustrates that when an LEU biomolecule is adsorbed onto C_{24}, the number of RDG points (about 0.8 on the y-axis) increases in highly attractive interaction locations. **Figure 5.9b-5.9d** show that there are Van der Waals (vdW) forces around ρ = 0 for C_{36}/LEU, C_{50}/LEU, and C_{70}/LEU complexes, which supports the physisorption nature of adsorption between them. Figure 9(a) shows that when the LEU biomolecule is adsorbed onto C_{24}, the number of RDG points (about 0.8 on the y-axis) rises, suggesting an increase in regions with extremely favourable contacts.

5.3.1.6 Sensing response

The opulence of a chemical sensor, which is dependent on the energy gap (EG), might theoretically be investigated with great insight utilising experimental sensing properties[57] . The EG can use the following equation to examine how changes in fullerene electronic properties effect changes in electrical conductivity or resistivity[58-60].

$$\sigma = AT^{3/2} \exp(-E_G/KT) \quad \ldots\ldots\ldots\ldots (4)$$

Where σ symbolises electrical conductivity, A a constant, K the Boltzmann constant, and T the operational temperature. In this section, we compute the sensing response with Eq. (4), which employs the formula to illustrate the efficacy of the sensing materials[61].

$$S = |(\sigma_1/\sigma_2)-1| = \exp(|\Delta E_G| / KT) - 1 \quad \ldots\ldots\ldots\ldots (5)$$

The complex and Fullerens energy gaps are described by E_{G2} and E_{G1}, respectively, where $E_G = E_{G2} - E_{G1}$.

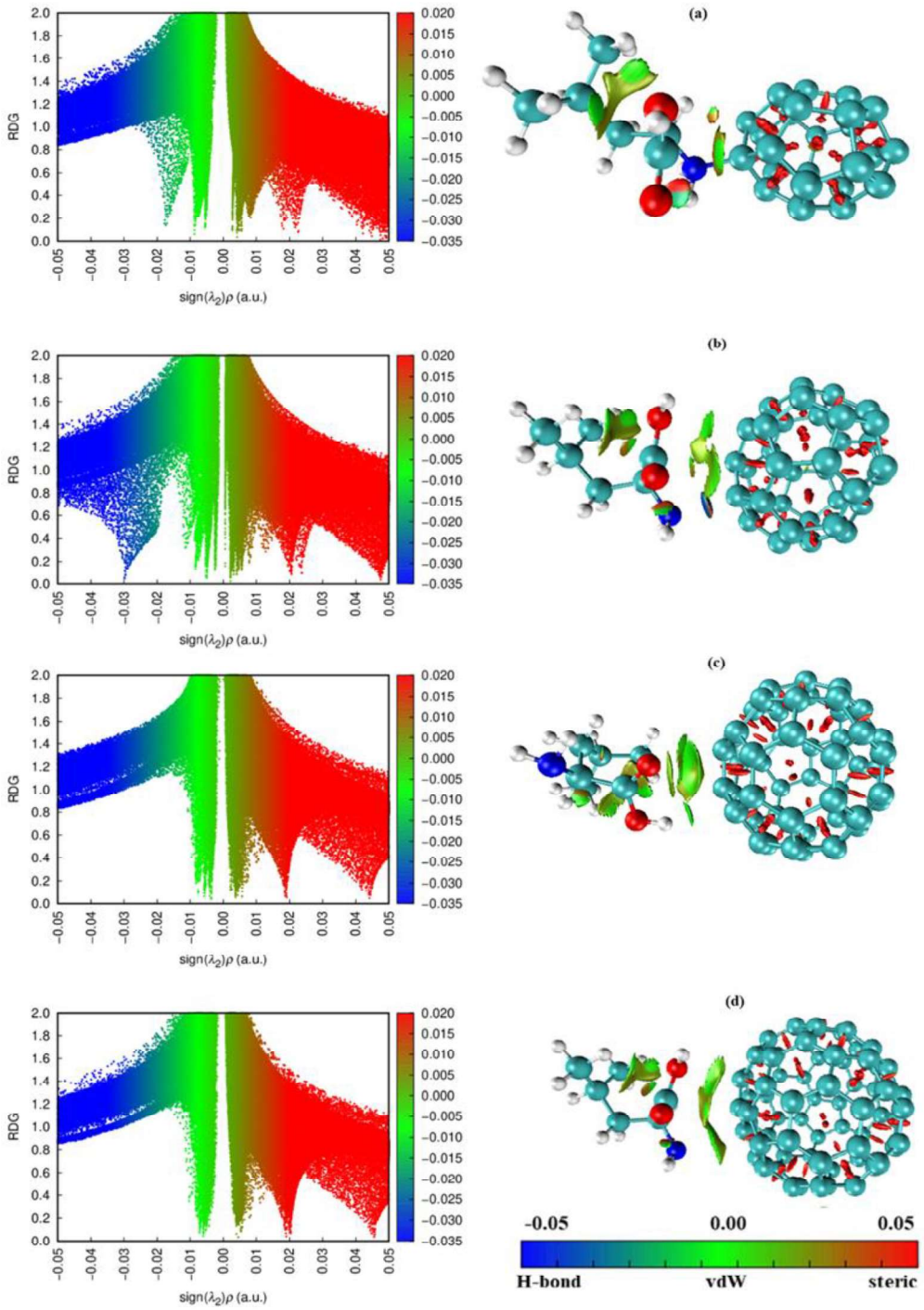

Figure 5.9: *The Reduced Density Gradient (RDG) scatter plots (Left) and Non-Covalent Interaction (NCI) isosurfaces (Right) of (a) C_{24}/LEU,(b)C_{36} /LEU, (c)C_{50}/LEU and(d) C_{70}/LEU respectively C,H,O, and N atoms are shown in light blue, white, red, and dark blue, respectively.*

The LEU biomolecule significantly altered the HOMO-LUMO band gap of the C_{24} fullerene (**Table 5.4**). As a result, LEU adsorption induces a significant change in the E_G of the

fullerene, demonstrating that the C_{24} is sensitive to the biomolecule LEU. According to our analysis, the best sensing response of all the systems considered for C_{24} fullerene to the LEU is around 8.45 at 310 K (**Table 5.4**). Because there is no noticeable change in EG after adsorption over the fullerenes, the sensing capabilities of the other complexes, C_{36}/LEU, C_{50}/LEU, and C_{70}/LEU, is substandard.

Table 5.4: *Calculated difference in E_G (ΔE_G), Recovery Time (τ) and Sensing Response(S) for LEU over C_{24},C_{36},C_{50} and C_{70} fullerene, respectively(T=310K).*

System	ΔE_G (eV)	τ (sec)	S
C_{24}/LEU	-0.06	3.42×10^{3}	8.45
C_{36} /LEU	0.03	4.9×10^{-10}	2.07
C_{50}/LEU	-0.02	2.31×10^{-10}	1.11
C_{70}/LEU	0.01	7.12×10^{-10}	0.45

5.3.1.8 Recovery time

Recovery time has been shown to be a critical parameter for chemical sensors that reflect the desorption process by heating the adsorbent to a higher temperature or exposing it to UV light, and it is significantly connected with the intensity of the contact. Higher interaction energies between molecules and an adsorbent extend the time it takes for them to recover and diminish their own interactions, making them less appropriate for use in sensing applications. As a result, a suitable sensor must have an acceptable optimal interaction energy and interaction distance[62]. The Recovery Time (τ) is given by the equation[63-64].

$$\tau = \upsilon_0^{-1} \exp(-E_{ad}/KT) \text{ ……..(6)}$$

Where T, K, and υ_0 represent temperature, Boltzmann's constant, and attempt frequency, respectively. Experiments have revealed that different photonic frequencies (υ_0) or thermal energy may be used to trigger the desorption of medications and proteins[63]. We calculated the recovery lengths for the LEU from the chosen fullerene's perimeter using a υ_0 of 10^{15} s^{-1} and a temperature of 310 K (See **Table 5.4**). We found that the highest recovery time for the LEU biomolecule is 3.42×10^{3} s , which is consistent with projections given the significant chemisorption nature of C_{24} fullerene. Because of the prolonged recovery time, the LEU biomolecule may be separated from the biological system using C_{24} fullerene. Even for

C_{36}/LEU, C_{50}/LEU, and C_{70}/LEU, the interatomic distance from the fullerene is 2.45 Å, 2.45 Å and 2.87 Å, respectively, and the recovery time is 4.9×10^{-10} s, 2.31×10^{-10} and 7.12×10^{-10} s indicating that the LEU may be used for the best detection when using the C_{36}, C_{50}, and C_{70} fullerenes.

5.3.1.8 Global indices

In order to further investigate the activity of fullerenes or biomolecular systems, we computed global index features such as Chemical potential (μ), Chemical hardness (η) and Electrophilicity (ω) (**Table-5.5**). The formula below gives the global indices parameters[62][65].

$$\text{Chemical Potential}(\mu) = -(I + A)/2 \quad \text{.....(7)}$$

$$\text{Hardness } (\eta) = (I - A)/2 \quad \text{.....(8)}$$

$$\text{Electrophilicity } (\omega) = \frac{\mu^2}{2\eta} \quad \text{.....(9)}$$

Where I = $-E_{HOMO}$ and A = $-E_{LUMO}$. Table 6 details the global indices tabulated using equations (8) through (10). Higher global hardness leads in more stable compounds, which is directly related to the chemical stability of the molecules. C_{70} is the most stable fullerene in our comparison, and the C_{70}/LEU complex is likewise the most durable. Following LEU adsorption over C_{50} and C_{70} fullerene, there has been no change, however following LEU adsorption over C_{24} and C_{36} fullerene, there has been an increase of +14.13% and +21.05%, respectively. Following the adsorption of an LEU biomolecule onto fullerenes, the HOMO and LUMO locations of the systems result in a considerable shift in chemical potential (μ). The values of change by -19.07%, -17.49%, -3.45%, and -3.58%, respectively, for LEU adsorbed on C_{24}, C_{36}, C_{50}, and C_{70} fullerene. It has been established that LEU/C_{24} displays the greatest change in chemical potential, suggesting their strong connection. Electrophilicity (ω) is the tendency of atoms or molecules to receive electrons. The pristine C_{24}, C_{36}, C_{50}, and C_{70} fullerenes had electrophilicity(ω) values of 14.35, 22.19, 20.96, and 9.33 eV, respectively, and the order of has altered by +42.58%, +43.75%, +6.77%, and +8.25% for LEU adsorption over selected fullerenes. When LEU is adsorbed on C_{24} and C_{36} fullerenes, a maximum change shows their significant interaction.

Table 5.5: *Global indices parameter of systems*

System	E_{LUMO} (eV)	E_{HOMO} (eV)	E_G (eV)	E_F (eV)	μ (eV)	η (eV)	ω (eV)
C_{24}	-4.22	-6.05	1.83	-5.14	-5.14	0.92	14.35
C_{36}	-4.46	-5.59	1.13	-5.03	-5.03	0.57	22.19
C_{50}	-4.57	-5.87	1.30	-5.22	-5.22	0.65	20.96
C_{70}	-3.66	-6.34	2.68	-5.00	-5.00	1.34	9.33
C_{24}/LEU	-3.15	-5.16	1.89	-3.88	-4.16	1.05	8.24
C_{36} /LEU	-3.46	-4.83	1.1	-4.58	-4.15	0.69	12.48
C_{50}/LEU	-4.39	-5.69	1.32	-5.21	-5.04	0.65	19.54
C_{70}/LEU	-3.45	-6.12	2.67	-4.89	-4.79	1.34	8.56

5.3.1.9 Solvent effect

The usefulness of biologically active molecules is governed by their structure and the intermolecular interactions they have with the solvent, which affect biological processes[66] . To completely comprehend biosensing systems, it is crucial to add solvent effects (the polarizable continuum model, or PCM approach) in DFT research. The intricate interactions between biomolecules, solvent molecules, and sensor surfaces have a major impact on binding affinities, sensing processes, and conformational changes[67]. We used the DFT/B3LYP/6-311(d,p) with D3 version of Grimme's dispersion to reoptimize each of the four fullerenes, the LEU biomolecule, and all of the minimal configurations of LEU and fullerenes complexes in the water solvent. **Table 5.6** displays the observed adsorption energies and sensor parameter values. The results show that the overall energy values of the LEU, C_{24}, and C_{36} systems decrease, resulting in a rise in the adsorption energies of the LEU/C_{24} and LEU/C_{36} complexes, which are -1.58 eV and -1.23 eV, respectively, compared to gaseous phase. As a result of the solvent's influence, the adsorption energy of the LEU/C_{50} and LEU/C_{70} complexes diminishes, resulting in a shorter recovery time in the aquatic environment and a reduced sensing response. Higher interaction energy in the aqueous environment predicts a greater sensing response and longer recovery time for the LEU/C_{24} and LEU/C_{36} complexes (see **Table 5.6**). In order to anticipate the solubility of the drug molecules in water, the solvation energies (E_{sol}) were computed using the following equation[68].

$$\Delta E_{sol} = E_{sol} - E_{gas} \quad \ldots\ldots\ldots\ldots\ldots\ldots(10)$$

where E_{sol} and E_{gas} indicate the energy of the system in the water solvent and gas, respectively. The observed E_{sol} for the LEU is -0.251 eV, while the measured E_{sol} for the C_{24} and C_{36} fullerenes is -0.025 eV and -0.089 eV, respectively. E_{sol} is discovered at -0.72 eV and -1.21 eV for the LEU/C_{24} and LEU/C_{36} complexes, respectively. It implies that the solvation energies of LEU complexes with C_{24} and C_{36} are less than the total of the solvation energies of LEU, C_{36}, and C_{24} fullerenes. These studies indicate the LEU, C_{24}, and C_{36} fullerenes' great water solubility and strong polarity. According to the electronic structures, the change in E_G for C_{24} and C_{36} fullerene by LEU in water is 0.12 and 0.27 eV higher than in the gas phase. As a consequence, the sensing response of the C_{24} and C_{36} fullerenes to the LEU increases from 8.45 and 2.07 in the gas phase to 843.2 and 11.6103 in water, showing that the biomolecule including the C_{24} and C_{36} is extremely sensitive in solvent medium. However, because of their similarly low sensing responses of 0.45, LEU/C_{50} and LEU/C_{70} interact less in the solvent effect.

Table 5.6: *Calculated value of Adsorption energy (E_{ad}), LUMO energy (E_{LUMO}), HOMO energy (E_{HOMO}), HOMO-LUMO gap (E_G), Recovery Time (τ) and Sensing Response (S) for LEU adsorbed C_{24},C_{36},C_{50} and C_{70} fullerene with solvent effect, respectively.*

System	E_{ad} (eV)	E_{LUMO} (eV)	E_{HOMO} (eV)	E_G (eV)	τ (sec)	S
C_{24}/LEU	-1.58	-3.15	-5.16	2.01	4.8×10^{10}	843.2
C_{36} /LEU	-1.23	-3.46	-4.83	1.37	9.94×10^{4}	11.6×10^{3}
C_{50}/LEU	-0.28	-4.39	-5.69	1.3	3.57×10^{-11}	0.45
C_{70}/LEU	-0.29	-3.45	-6.12	2.67	5.19×10^{-11}	0.45

5.3.2 Molecular dynamics simulation results

A notable approach is molecular dynamics simulation, which allows for the explicit maintenance of equilibrium and stability for biomolecule and fullerene complexes in an aqueous environment, precisely at 310 K. In the previously described DFT-PCM study, we revealed that biomolecules' sensitivity to fullerenes increases in a water environment, which also enhances the sensing response of C_{24} and C_{36} fullerenes compared to the gaseous phase. Additional investigation is needed to better understand the dynamical stability of complexes in

a water environment. In this section, we calculated the temperature, total energy, and root mean square deviation (RMSD) of the LEU/C_{24} and LEU/C_{36} complexes up to 50 ns.

Table 5.7: *Detail of the simulation boxes which used in this work*

System	No. of LEU Bio-molecules	No. of fullerenes	No. of water molecule	Dimension of the cubic box(nm)
C_{24}/LEU	2	4	5676	5.6 × 5.6 ×5.6
C_{36} /LEU	2	4	7760	6.2× 6.2 ×6.2

A careful examination of the RMSD curves reveals that there was very little divergence (approximately 4-5 nm) during the 50 ns trajectory for the all-equilibrated systems. In comparison to LEU/C_{36}, the LEU/C_{24} system had the lowest variance in RMSD during the duration of the simulation. The radial distribution (RDF) or g(r) between the biomolecule and C_{24}, C_{36} fullerenes has been studied to understand how biomolecules are dispersed throughout the surfaces of C_{24} and C_{36} fullerenes in aqueous solutions for the two systems. **Figure 11**(b) shows this distribution. It should be noted that the centers of gravity for fullerenes and biomolecules are shown in the two figures. Because of the strong repulsive interactions that occur between biomolecules and fullerenes, we may deduce from the RDF graphs that g(r) is zero across short distances. Because of the higher steric influence of the LEU molecules, g(r) for the LEU/C_{24} system began to be nonzero at greater distances than that for the LEU/C_{36} system. Because LEU biomolecules have higher interaction energies with C_{24} and C_{36} fullerenes, which is consistent with DFT/PCM investigations, LEU biomolecules are more likely to be detected around these fullerenes. The biomolecules are scattered in the range of 0.2-2.5 nm around the C_{24} and C_{36} fullerene surfaces, as shown in Figure 11(b). The RDF findings show that the adsorbed biomolecules and C_{24}, C_{36} fullerene interact strongly at a distance of 0.5 nm in all conditions. Finally, **Figures 12** (a) and (b) show the variation of total energy and temperature as a function of simulated time steps for the LEU/fullerene complexes. We observe that the overall energies of the two complexes reach equilibrium during the simulation time. The temperature fluctuation graph shows that the simulation temperature, or

310K, was maintained throughout the experiment for all complexes. These findings show that the complexes reach equilibrium and adsorption occurs at room temperature for 50 ns.

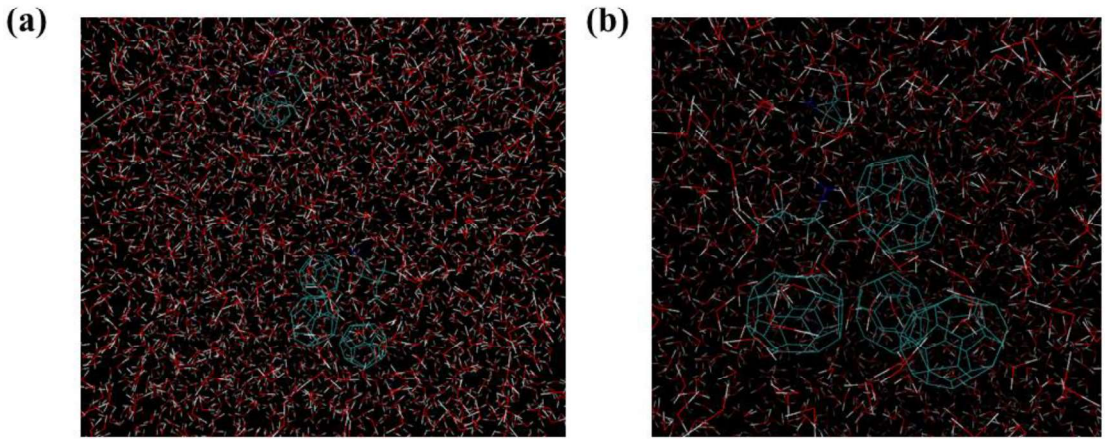

Figure 5.10: *Snapshots for (a) C_{24}/LEU and (c)C_{36}/LEU simulation systems.*

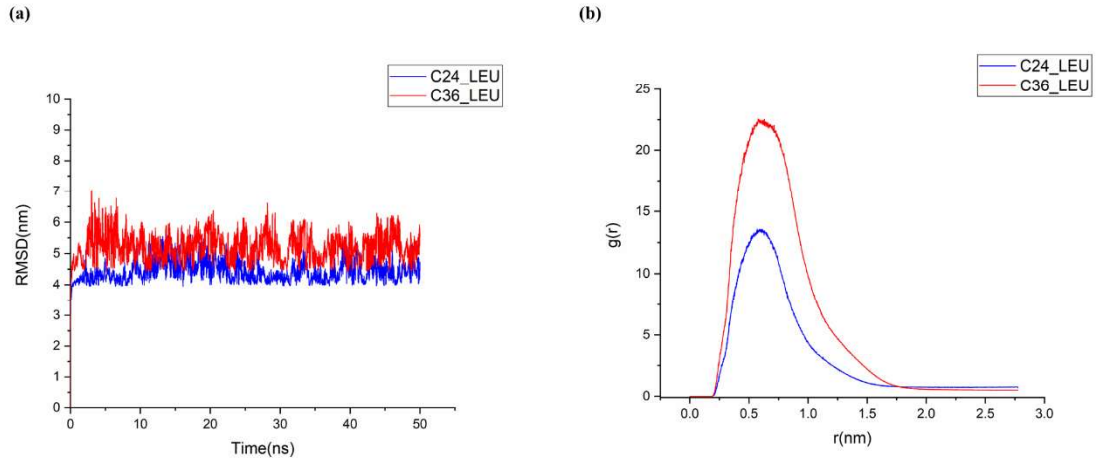

Figure 5.11: *(a)RMSD curves for the interacted LEU biomolecule and C_{24} ,C_{36} fullerene as a function of time and (b)comparison of radial distribution (g(r)) of biomolecules around the C_{24} and C_{36} fullerene surfaces versus distance.*

The derived total energy plots for the LEU/C_{24} and LEU/C_{36} complexes, shown in Figure 12(a), show that these complexes are more stable in water, with maximum average total energies of roughly -170000 and -230000 KJ/mol, respectively, which agree with the DFT/PCM results.

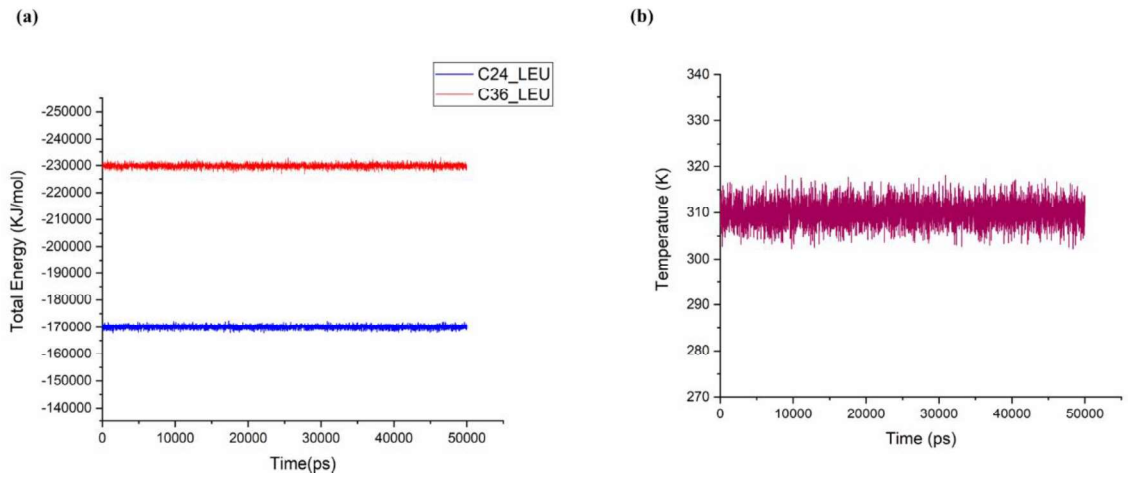

Figure 5.12: *MD simulation plots for the (a) Total Energy and (b) Temperature for the biomolecules/fullerenes against the time simulation.*

5.4 Conclusions

In this study, the DFT-D3 approach in conjunction with solvent was utilized to investigate and evaluate the adsorption mechanism process of the LEU biomolecule on C_{24}, C_{36}, C_{50}, and C_{70} fullerenes. Our findings indicate that the LEU and C_{24} fullerene interact significantly in the gas phase, resulting in a stronger sensing response and a longer recovery time. As a result, utilizing C_{24} fullerene as a biosensor, the biomolecule LEU may be separated from other amino acid sequences. Because of the physisorption property of LEU adsorption on C_{36}, C_{50}, and C_{70} fullerene, reduced recovery durations in the 10^{-10} s range are observed, as well as an appreciable sensing response. The optimal interaction energies and shorter interatomic distances between LEU biomolecules and C_{36}, C_{50}, and C_{70} fullerene imply a potential fullerene-based LEU detector. Furthermore, because of the solvent effect, the adsorption energy of LEU/C_{24} and LEU/C_{36} complexes is greater in the solvent phase than in the gaseous phase, making them more reactive and persistent in a water environment. The C_{24} and C_{36} fullerenes significantly accelerate sensory responses and recovery times. As a result, C_{24} and C_{36} fullerene may remove the LEU biomolecule from the biological systems in the aqueous phase. The interaction energy of LEU with C_{50} and C_{70} reduces as a result of the solvent effect, indicating that the LEU/C_{50} and LEU/C_{70} complexes are less reactive and their usage in LEU detection may be limited. According to a detailed classical molecular dynamics simulation, the LEU/C_{24} and LEU/C_{36} complexes are well equilibrated and astonishingly stable in the aqueous environment condition at ambient temperature (310K). Furthermore, the RDF plots show that the biomolecules are

equally distributed at observable distances across the C_{24} and C_{36} fullerene, lending credence to the adsorption mechanisms hypothesized from the DFT results.

Finally, using a combination of DFT and MD simulation results, we concluded that C_{24} and C_{36} fullerenes may be an excellent alternative for developing new-generation high performance biomolecule functionalization and sensors in a water environment at room temperature.

References:

1 J. . Allemand, P.M., Khemani, K.C., Koch, A., Wudl, F., Holczer, K., Donovan, S., Grüner, G. and Thompson, *Science (80).*, 1991, **253**, 301–302.

2 H. Kroto, *Science (80).*, 1988, **242**, 1139–1145.

3 D. E. M. Fowler, Patrick W., *An Atlas of Fullerenes*, 2007.

4 A. M. L, 2011, **10**, 1305–1318.

5 C. A. Celaya, L. F. Hernández-Ayala, F. Buendía Zamudio, J. A. Vargas and M. Reina, *J. Mol. Liq.*,10.1016/j.molliq.2021.115528.

6 S. K. Jana, D. Chodvadiya, N. N. Som and P. K. Jha, *Diam. Relat. Mater.*, 2022, **129**, 109305.

7 S. F. Species, 1986, **128**, 501–503.

8 Y. A. Wang, 2006, 1–11.

9 Susumu Saito and Atsushi Oshiyama, *Phys. Rev. B*, 1991, **44**, 532–535.

10 M. B. Javan, N. Tajabor, M. R. Roknabadi and M. Behdani, *Phys. E Low-dimensional Syst. Nanostructures*, 2011, **43**, 1351–1359.

11 R. F. C. and R. E. S. H.W.Kroto, J.R.Heath, S.C.O'Brien, *Nature*, 1985, **318**, 162–163.

12 P. S. S. Mehta, Goverdhan, *etrahedron Lett.*, 2002, **43**, 9343–9346.

13 H. W. Karoto, *Nature*, 1987, **329**, 529–531.

14 Z. Chen and A. Hirsch, 2002, 121–135.

15 J. R. Heath, 1998, **393**, 730–731.

16 C. Piskoti, J. Yarger and A. Zettl, *Nature*, 1998, **393**, 771–774.

17 F. Naderi, S. Rostamian and B. Naderi, 2012, **7**, 2006–2009.

18 V. A. Online, *RSC Adv.*, 2016, **6**, 78176–78180.

19 J. L. Head-Gordon, *PCCP*, 2019, **21**, 4763–4778.

20 I. Introduction, 2003, **30**, 30–33.

21 A. Barre, R. Culerrier, C. Granier, L. Selman, W. J. Peumans, J. Bienvenu and P. Rougé, 2009, **46**, 1595–1604.

22 B. T. Tomić, C. S. Abraham, S. Pelemiš, S. J. Armaković and S. Armaković, *Phys. Chem. Chem. Phys.*, 2019, **21**, 23329–23337.

23 V. Mahamiya, A. Shukla and B. Chakraborty, 2022, **897**, 1–6.

24 Z. Bagheri, *Appl. Surf. Sci.*, 2016, **383**, 294–299.

25 K. Kalantar-zadeh, J. Z. Ou, T. Daeneke, M. S. Strano, M. Pumera and S. L. Gras, 2015, 5086–5099.

26 Y. Wang, S. Yang, M. Fuentes-cabrera, S. Li and W. Liu,10.1021/jacs.7b01216.

27 K. Liu, J. Feng, A. Kis and A. Radenovic, 2014, 2504–2511.

28 S. Pilehvar and K. De Wael, .

29 A. Meller, T. Israel, S. A. Meller and M. W. Grinstaff, *Chem Soc Rev*, 2018, **47**, 8512–8524.

30 H. D. Niall, *Methods Enzymol.*, 1973, **27**, 942–1010.

31 P. J. Garlick, *J. Nutr.*, 2005, **135**, 1553S-1556S.

32 and S. M. H. Ananieva, Elitsa A., Jonathan D. Powell, *Adv. Nutr.*, 2016, **7**, 798S-805S.

33 et al Yang, Jichun, *Nutr. Rev.*, 2010, **68**, 270-279.

34 and E. L. P. Kelly, Beth, *Cell Metab.*, 2020, **32**, 154-175.

35 et al Wang, Xiaotian, *Front. Cell. Neurosci.*, 2023, **16**, 1060712.

36 D. P. Puliyanda, W. E. Harmon, M. J. Peterschmitt, M. Irons and M. J. G. Somers, 2002, 239–242.

37 S. Grimme, J. Antony, S. Ehrlich and H. Krieg, *J. Chem. Phys.*, , DOI:10.1063/1.3382344.

38 et al. M. J. Frisch, Trucks, G.W., Schlegel, H.B., Scuseria, G.E., Robb, M.A., Cheeseman, J.R., *Gaussian 09, Revis. A.02, Gaussian, Inc.*, 2016, 1–2.

39 H. J. C. Berendsen, D. van der Spoel and R. van Drunen, *Comput. Phys. Commun.*, 1995, **91**, 43–56.

40 A. D. Mackerell, N. Banavali and N. Foloppe, *Biopolymers*, 2001, **56**, 257–265.

41 P. Mark and L. Nilsson, *J. Phys. Chem. A*, 2001, **105**, 9954–9960.

42 G. Bussi, D. Donadio and M. Parrinello, *J. Chem. Phys.*, , DOI:10.1063/1.2408420.

43 B. Hess, H. Bekker, H. J. C. Berendsen and J. G. E. M. Fraaije, *J. Comput. Chem.*, 1997, **18**, 1463–1472.

44 T. Darden, D. York and L. Pedersen, *J. Chem. Phys.*, 1993, **98**, 10089–10092.

45 K. S. William Humphrey, Andrew Dalke, *Jounal Mol. Graph.*, 1996, **14**, 33–38.

46 C. Liang, J. Yang, C. Hao, S. Li, Y. Li and Y. Jin, 2008, **851**, 342–347.

47 X. Lu, Z. Chen, W. Thiel and P. Von Rague, *JACS*, 2004, **126**, 14871–14878.

48 M. Li, Y. Wei, G. Zhang, F. Wang, M. Li and H. Soleymanabadi, *Phys. E Low-dimensional Syst. Nanostructures*,10.1016/j.physe.2019.113878.

49 W. Qin, X. Li, W. W. Bian, X. J. Fan and J. Y. Qi, *Biomaterials*, 2010, **31**, 1007–1016.

50 M. Yoosefian and N. Etminan, *Amino Acids*, 2018, **50**, 653–661.

51 S. K. Jana, N. N. Som and P. K. Jha, *J. Mol. Liq.*, 2023, **383**, 122084.

52 R. Chandiramouli, A. Srivastava and V. Nagarajan, *Appl. Surf. Sci.*, 2015, **351**, 662–672.

53 S. Demir and M. F. Fellah, *Appl. Surf. Sci.*, , DOI:10.1016/j.apsusc.2019.144141.

54 T. Zubatiuk, G. Hill, D. Leszczynska, M. Fan, A. H. Rony and J. Leszczynski, *Chem. Phys. Lett.*, 2018, **706**, 708–714.

55 E. R. Johnson, S. Keinan, P. Mori-Sánchez, J. Contreras-García, A. J. Cohen and W. Yang, *J. Am. Chem. Soc.*, 2010, **132**, 6498–6506.

56 M. Kurban and İ. Muz, *J. Mol. Liq.*,10.1016/j.molliq.2020.113209.

57 A. Ahmadi Peyghan, N. L. Hadipour and Z. Bagheri, *J. Phys. Chem. C*, 2013, **117**, 2427–2432.

58 P. Dipak, D. C. Tiwari, A. Samadhiya, N. Kumar, T. Biswajit, P. A. Singh and R. K. Tiwari, *J. Mater. Sci. Mater. Electron.*, 2020, **31**, 22512–22521.

59 D. C. Tiwari, P. Atri and R. Sharma, *Synth. Met.*, 2015, **203**, 228–234.

60 N. Illyaskutty, H. Kohler, T. Trautmann, M. Schwotzer and V. P. M. Pillai, *J. Mater. Chem. C*, 2013, **1**, 3976–3984.

61 Y. Yang, A. Sun and M. Eslami, *Phys. E Low-dimensional Syst. Nanostructures*, 2021, **125**, 114411.

62 M. A. Hossain, M. R. Hossain, M. K. Hossain, J. I. Khandaker, F. Ahmed, T. Ferdous and M. A. Hossain, *Chem. Phys. Lett.*, 2020, **754**, 137701.

63 H. Rahman, M. R. Hossain and T. Ferdous, *J. Mol. Liq.*, 2020, **320**, 114427.

64 N. A. Tukadiya, S. K. Jana, B. Chakraborty and P. K. Jha, *Surfaces and Interfaces*, 2023, **41**, 103220.

65 S. Vadalkar, D. Chodvadiya, N. N. Som, K. N. Vyas, P. K. Jha and B. Chakraborty, *ChemistrySelect*,10.1002/slct.202103874.

66 N. Etminan, M. Yoose, H. Raissi and M. Hakimi,10.1016/j.molliq.2015.12.009.

67 M. Cossi, V. Barone, R. Cammi and J. Tomasi, *Chem. Phys. Lett.*, 1996, **255**, 327–335.

68 J. Jiang, T. Yan, D. Cui, J. Wang, J. Shen, F. Guo and Y. Lin, *J. Mol. Liq.*, 2020, **315**, 113741.